Materials Science, *Vol. 21*, *No. 3*, *2003*

Combined SNOM/AFM microscopy with micromachined nanoapertures

JACEK RADOJEWSKI[1*], PIOTR GRABIEC[2]

[1]Faculty of Microsystem Electronics and Photonics, Wrocław University of Technology, Wybrzeże Wyspiańskiego 27, 50-370 Wrocław, Poland

[2]Institute of Electron Technology, al. Lotników 32/46, 02-668 Warsaw, Poland

We describe a new combined SNOM/AFM cantilever probe with the aperture FIB micromachined in a hollow metal pyramid fabricated on its end. The cantilever can be used in a microscopy set-up with the optical or piezoresistive AFM detection system. A processing sequence proposed in the article offers a high reproducibility in batch processing typical of semiconductor technology. Moreover, the angle of the apex cone is close to 50° which renders it possible to obtain a high-aperture optical throughoutput. The probe construction, manufacturing and its basic optical parameters are described.

Key words: *AF; SNOM microscopy; cantilever technology; nanoaperture*

1. Introduction

The concept of the near-field optical microscopy (SNOM) was first published by Synge [1] in 1928. In 1984 Pohl et al. [2] and Lewis et al. [3] used this technology in practice. Since that time many authors have reported their SNOM systems, mainly based on optical waveguides with the nanoaperture fabricated on the end much smaller than the light wavelength λ [4, 5]. The tips usually used in this method are tapered optical fibres coated with metal films in such a way that the very end of the tip is free of the metal layer. The use of nanoaperture as a local probe makes it possible to overcome the $\lambda/2$ diffraction limit which occurs if the light is detected in far field, i.e., when the detector distance is much larger than the wavelength λ of the light used in the experiment. In SNOM systems such a local probe is raster-scanned over the sample surface at a distance much smaller than λ. A simultaneous detection of transmitted, reflected or scattered light makes it possible to image optical properties of the sample.

*Corresponding author, e-mail: jacek.radojewski@pwr.wroc.pl.

The main drawback of the tapered-fibre based SNOM systems is the resolution limited by 'shear force' mechanism used to control sample–tip distance [6]. This technique uses an optical fibre probe vibrating parallel to the surface under the test in its dominant mechanical resonance. The vibration amplitude is a few nanometres. The amplitude and phase change due to tip–surface distance variation is used for the distance regulation. Unfortunately, the fabrication process of tapered fibres renders very small angles of the apex resulting in a significant squeezing of the light passing through the tapered region and the aperture itself and consequently in a relatively low throughoutput of the aperture.

In the present paper, we demonstrate a novel technology of combined SNOM /AFM cantilever. Our earlier approach [7] allowed fabrication of a piezo-SNOM/AFM probe but the reproducibility of the process and optical quality of the device were unsatisfactory. In this paper, we report an innovative processing sequence with direct FIB aperture drilling. It offers highly reproducible batch processing, typical of the semiconductor technology and renders it possible to produce cantilevers playing the role of AFM detectors as well as nanoaperture detectors. Moreover, the illumination of the aperture is easier because of wide input opening and its large cone angle. The throughoutput is in the range of 10^{-5} and higher for aperture diameter of 50 nm.

Apertures in hollow pyramids have been formed by a direct ion beam drilling with a focused beam of 30 keV Ga^+ ions. Direct FIB drilling is a reproducible process for hole formation in the 30–100 nm diameter range. Formation of smaller apertures is possible if special FIB drilling/deposition procedure is applied. Our apertures possess excellent optical properties making it possible to use them in polarization-dependent experiments, as was suggested by Betzig et al. [8], Valaskovic et al. [9] and Husler et al. [10]

2. SNOM/AFM cantilever technology

Based on our experience and having considered examples reported in the literature [11, 12], we have developed an innovative processing sequence, which offers a highly reproducible batch processing, typical of semiconductor technology and silicon micromechanics rendering it possible to produce cantilevers playing the role of AFM detectors as well as optical photo-detectors or nanoaperture detectors.

A number of functional components were integrated in one silicon chip to form the microprobe. The microprobe forms a cantilever beam with a hollow pyramid at the end. A set of force sensitive piezoresistors, placed in the base of the beam, allows detection of small deflections of the beam. A tip-shape platform acts as an atomic force sensitive unit, while a nano-hole in the platform serves for near field optical measurements.

The fabrication process starts from pad oxide formation followed by LPCVD nitride deposition. Then a rectangular mesa in a future beam area is defined and plasma

etched (Fig. 1a). The mesa level remains elevated several micrometers over the whole surface. Next, a sequence of oxidation, photolithography and implantation is used to form a set of piezoresistors in the base of the beam area (Fig. 1b). The post -implantation oxidation is optimized to protect effectively the probe surface against later etching processes. In the next step, membrane areas are defined in the nitride film at the back sides of the wafer, and subsequently etched in hot KOH solution while the front side of the wafer is protected by a special chuck. The membrane thickness of 30 μm (as measured in the thickest part, i.e. in the mesa area) is achieved by etching (Fig. 1c). In the following sequence an inverse hollow pyramid is created.

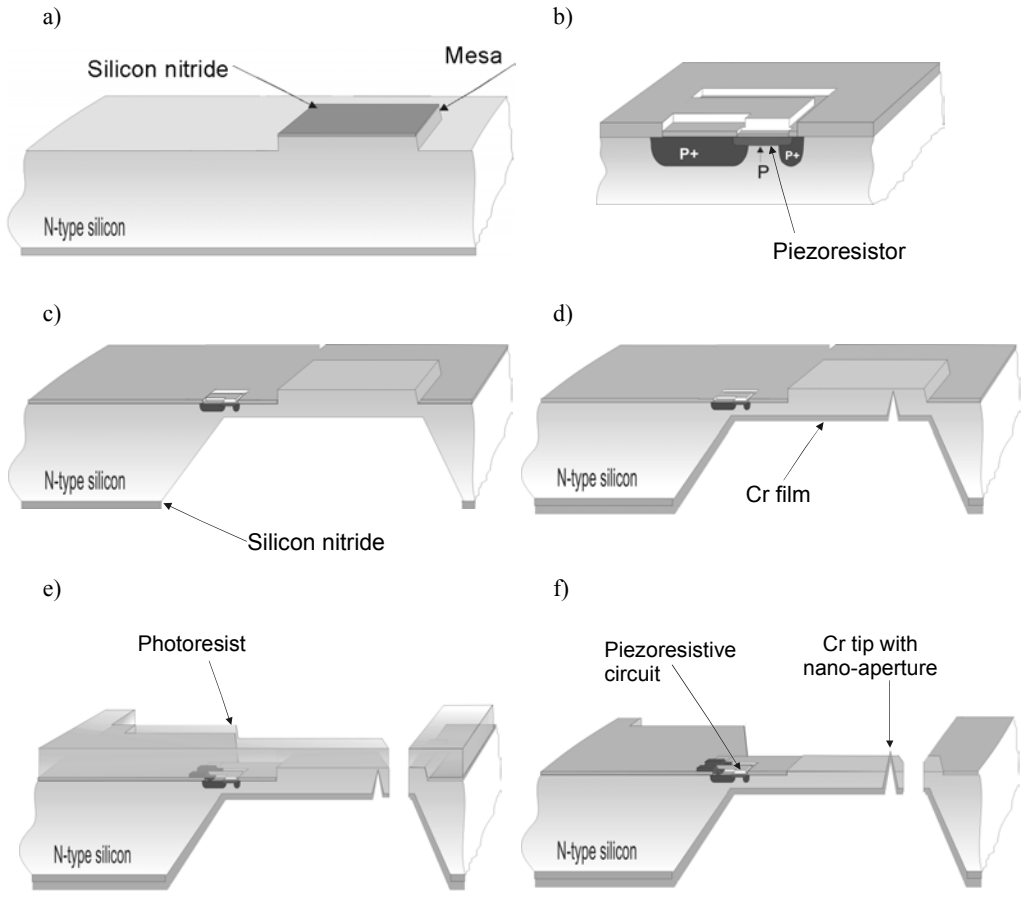

Fig. 1. Scheme of the process sequence of the microprobe fabrication. See text for details

First, a thin nitride layer is LPCVD deposited. A square contour is photolitho-graphically defined at the back side of the membrane, in the future tip location, using SU-8 process followed by thick oxidation, resulting in a LOCOS-like shape. Next, both the nitride and oxide layers are dry etched away from the square area on the back

side of the membrane. Finally, an inverse pyramid hollow is etched in this place where bare silicon was previously exposed. Photolithographic opening of contacts to piezoresistors, followed by the creation of metal connections in standard CMOS IC's processing sequence, completes the formation of the piezoresistor set. Then, the back side of the membrane, including pyramid walls, is covered with chromium layers in magnetron sputtering process (Fig. 1d). In the next step, the probe shape is photolithographically defined at the front side of the wafer, followed by silicon plasma etching and chromium etching (Fig. 1e). Finally, a mask-less plasma etching of the nitride /pad oxide sandwich from the top of the mesa structure is performed, followed by a deep plasma silicon etching, resulting in exposition of the metal pyramid in the former mesa area (Fig. 1f). SEM images of the main microprobe regions are shown in Fig. 2.

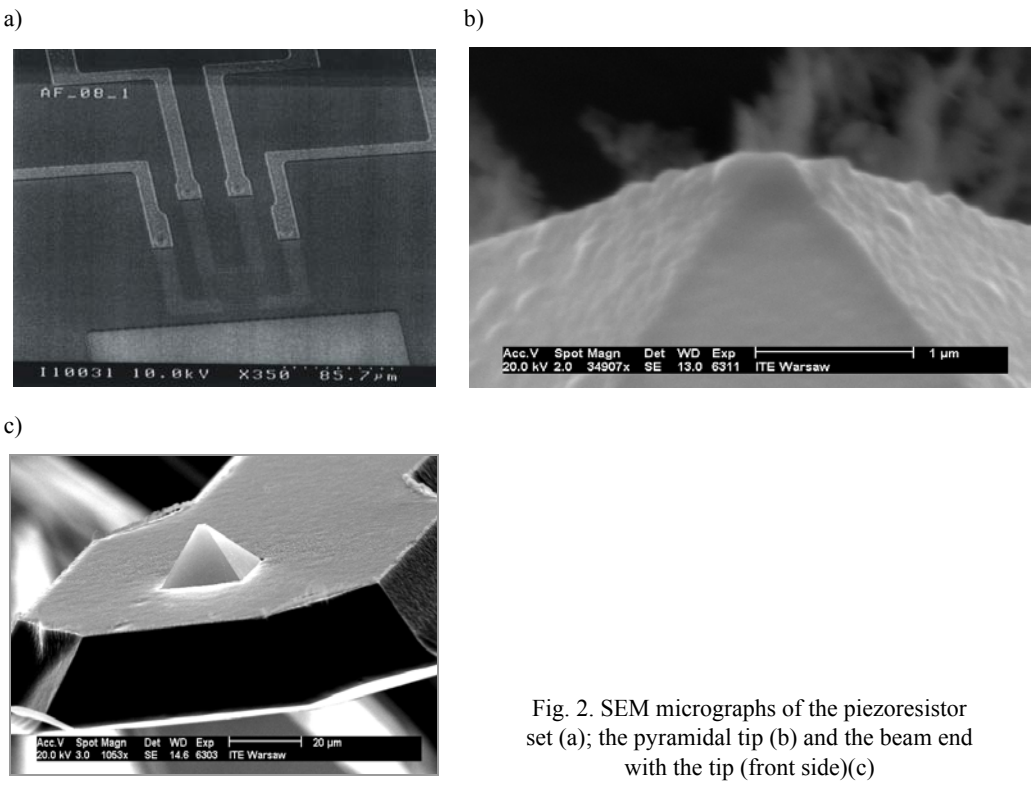

Fig. 2. SEM micrographs of the piezoresistor set (a); the pyramidal tip (b) and the beam end with the tip (front side)(c)

Creation of a small aperture of several tens of nanometres is the last step of the SNOM/AFM microprobe fabrication. A FIB direct ion beam drilling with a focused beam of 30 keV gallium ions is applied to produce a hole in the hollow chromium pyramid tip. The direct FIB drilling is a reproducible process for a hole formation in the 30–100 nm diameter range (Fig. 3). The ion dose for sputtering the hole is about 2×10^9 ions. The positions of specimens in regular arrays can be dialed in automatically, enabling a rapid processing of the samples. The FIB drilling experiments

indicate an aspect ratio limit of about 5:1 but the hole size is independent of the aspect ratio for holes of diameters below 100 nm. The available FIB systems equipped with an *xy*-stage and image recognition allows drilling 360 sensor Cr pyramids on the wafer at a reasonably short time with an excellent reproducibility (size deviation and

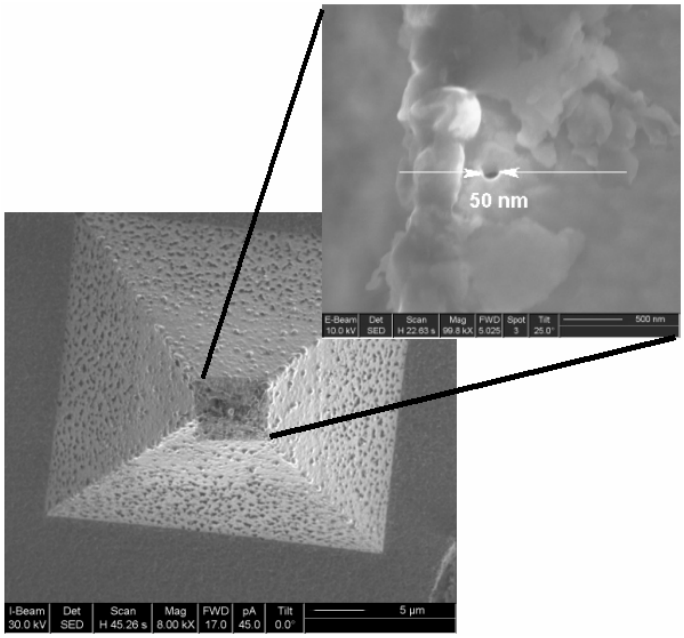

Fig. 3. SEM image of the tip shape
and the aperture obtained by the FIB method

circularity). For the beam geometry of l = 600 μm, b = 210 μm and d = 15 μm we obtained cantilevers with the spring constant k = 113 N/m and the resonance frequency f_r = 50 kHz.

3. Aperture verification

Looking at the SEM images of the tips etched by the FIB method described above (Fig. 3), one can see a well defined aperture on the end face of the pyramidal shaped tip, placed on the end of the piezoelectric cantilever. For a final verification of our tips, we performed polarization measurements of the aperture. For this purpose, we used helium-neon laser light (λ = 0.6328 μm) with the beam power of P = 5 mW. The light beam was coupled to the aperture via a microscopic objective of NA = 0.5. We used a $\lambda/4$ plate to convert the linear polarization of the incident light into the circular one, in order to have a possibility to control the input light polarization via a polarizer. The degree of polarization of the light which passed the nanoaperture was tested by an

analyzer placed between the aperture and the photomultiplier. A dummy sample was used in close proximity to the aperture for field conversion purpose (Fig. 4).

From the theoretical point of view [13], an ideally symmetrical aperture possesses two peaks of intensities associated with depolarization fields. They are generated in the regions where the incident field is normal to the core/coating interface. The depolarization field rotates following the orientation of the incident light polarity. As a result, a symmetrical behaviour should be observed in far field for symmetrical apertures. An elliptical or rough rim of aperture coming from metal grains strongly changes the field distribution resulting in an asymmetry in far field [14].

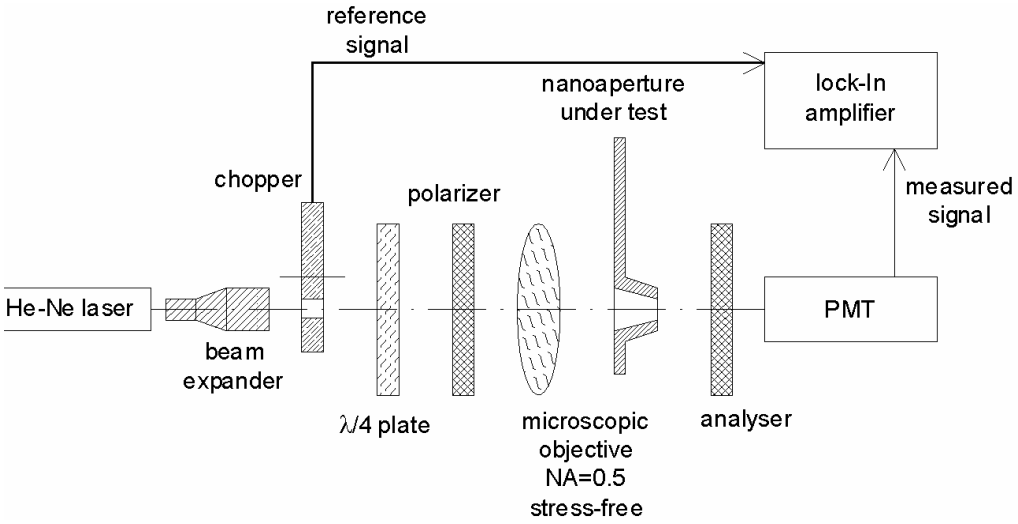

Fig. 4. Set-up for measurements of the polarization behaviour of fabricated apertures

a) b)

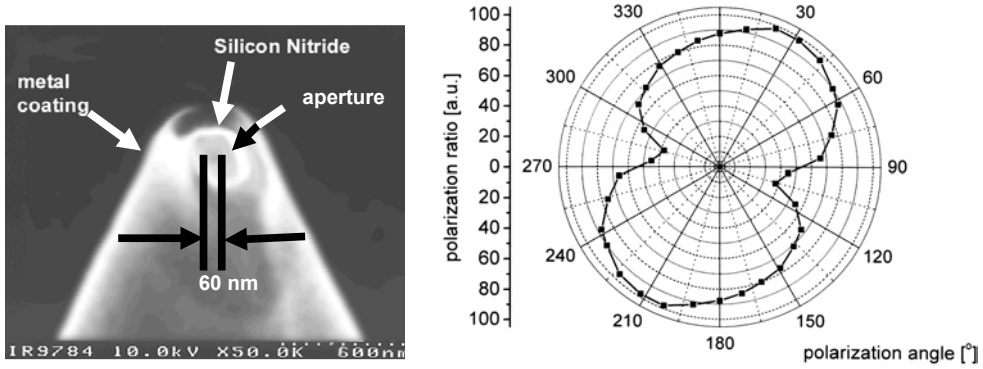

Fig. 5. SNOM nanoaperture probe from the authors' laboratory [7] (a) and a polarization ratio of 60/80 nm aperture with elliptical shape (b)

In the beginning of our measurements, we tested cantilevers described in [7], elaborated in this laboratory in 2001. After precise measurements of aperture we found an elipticity in its shape. In Fig. 5a, a SEM image of the 60/80 nm tip aperture, and in Fig. 5b – the corresponding polarization ratio graph are shown. We found that the minimum polarization ratio was about 1:38 and the maximum exceeded 1:98. After improving our technology, we expected to obtain better results (minimum to maximum polarization ratio difference factor less than two) due to a better circularity of the aperture opening. In Fig 6a, a relative polarization ratio for the aperture fabricated using our new batch technology is presented. In this case, we found the polarization ratio between 1:77 and 1:98. Thus, a significant improvement of optical properties of our SNOM cantilevers was confirmed.

a)

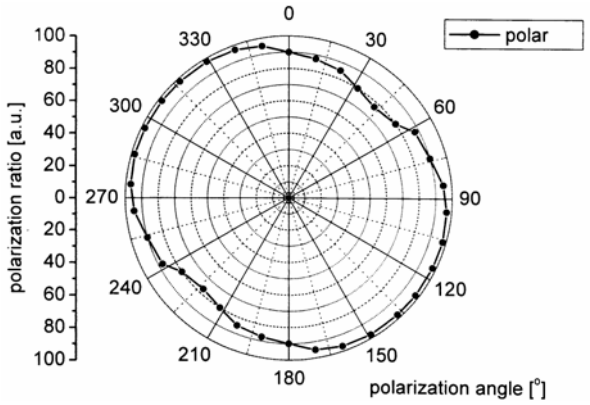

b)

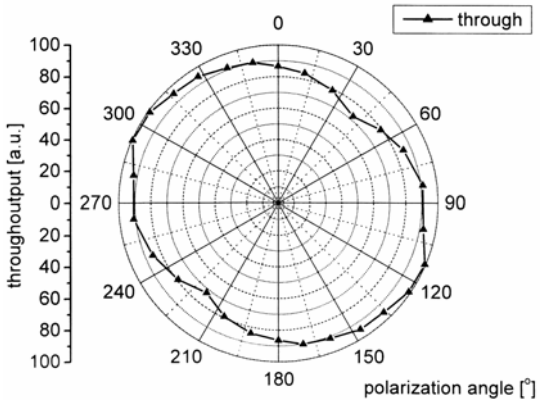

Fig. 6. Normalized polarization ratio of 50 nm aperture fabricated with the improved technology (a) and relative throughoutput of the 50 nm aperture (b)

The transmission coefficient of the apertures shows a strong dependence on its diameter. For example, for the cone angle 50° it is of the order of 10^{-3} for the aperture diameter of 100 nm, decreasing to 5×10^{-7} for the aperture diameter of 10 nm [15]. In our case, we obtained a 50-nm aperture throughoutput ratio of 5×10^{-5} with the values lying within 30% with respect to the polarization direction (Fig. 6b).

4. Microscope measurements

4.1. Microscope set-up

The measuring set-up of our SNOM microscope (Fig. 7) consists of two parts. One is a head support with a piezotable (PXY100, Piezojena) used for fine sample movement (scanning) in the *XY* plane (up to 100×100 μm). The piezotable can be additionally moved in the *XY* plane by means of two DC motorized micrometric screws (Owis). These coarse movements, which can be done on the distances of 5×5 mm, are used to select a place of interest over the sample for the subsequent precise scanning. The head standing on three legs on the head support can be rotated with respect to the sample fixed by *Z* fine movement piezostack to the fine *XY* movement piezotable. One of these legs is a DC motorized micrometric screw which is used to perform coarse *Z* movements of the head (cantilever) with respect to the sample. A fine *Z* movement is realized by the piezostack *Z* mentioned above. The cantilever bending due to force interactions with the sample surface is detected by a standard technique using the light reflected from the cantilever surface and detected by a quadrant detector. For the cantilever in position of a desired interaction force, the light spot is centred on the detector in such a way that the photocurrents from each quadrant are equal. Any movement of the cantilever, detected as a current imbalance signal, is used in a closed feedback loop with the *Z* piezostack to stabilize the interaction force during the scanning. Laser light used for this purpose is supplied via a monomode waveguide coupled to a 780 nm, 5 mW laser by *XYZ* precise single mode fibre coupler (Thorlabs). The laser is mounted in TEC with precisely controlled temperature by a TEC 2000 controller with the temperature stability of 1 mK. The laser power is controlled by a LDC 500 laser driver with 1 μW optical power resolution (Thorlabs). The light bundle from the waveguide end-face is focused by a lens system on the cantilever surface near the aperture. The position of light spot is regulated by an *XY* adjusting system which moves the fibre end with respect to the head body. The fibre is fixed inside a ceramic ferrule, cleaved and polished according to a standard procedure used during the FC/ST fibre connectors fabrication. The second laser light source (S1FC635 fibre coupled laser source) with 3-mW light power and λ = 635 nm, used for the aperture illumination, is coupled to the microscope head via another monomode fibre placed inside the same ferrule, parallel to the first one. The distance of the core centres of two fibres is 125 μm. The spot of 635 nm light is placed directly

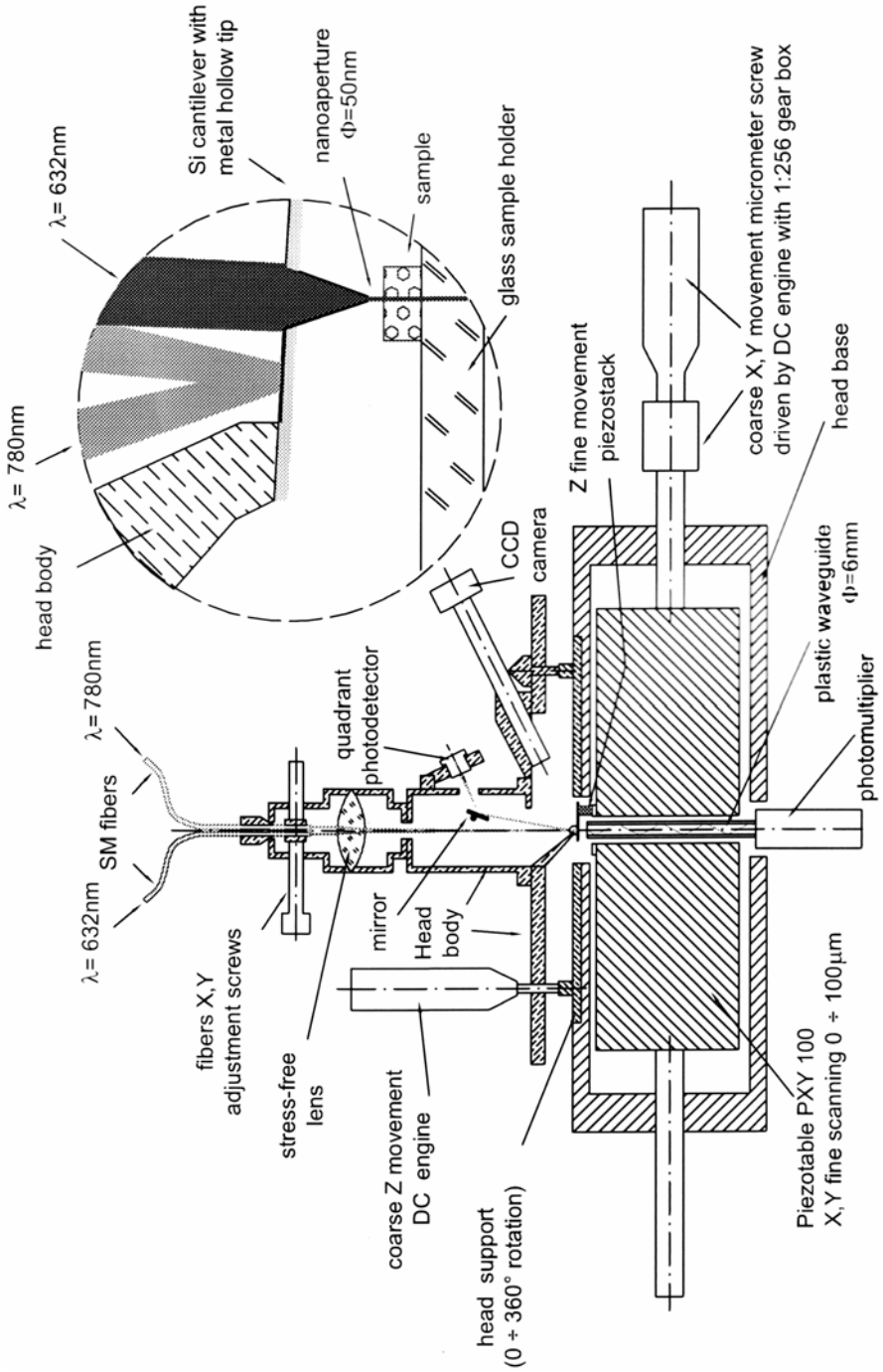

Fig. 7. SNOM/AFM microscope set-up

on the aperture entrance whereas the 780 nm light spot is placed nearby on the cantilever surface using the same lens and the *XY* ferrule adjusting system. The SNOM signal in the transmission mode is collected by a photomultiplier (Hamamatsu) placed under the head support. Light from the nanoaperture, after interacting with the sample surface, is coupled to one end face of 6 mm thick polycarbonate rod placed directly under the sample while the second end of the rod is coupled with the photomultiplier. The rod is passed through the head support via a PXY 100 table opening. The microscope head is connected to a scanning and acquisition electronic system controlled by a PC computer equipped with the ADDA measuring card (DAS 1702 ST-DA, Keithley) and an appropriate software (proximity control, scanning control + image processing) written in our laboratory under the C++ language.

4.2. Results

We performed test measurements using standard latex sphere samples for AFM and optical transmission contrast capability of our system. All experiments were taken in the constant height mode. In this way images are not topography-related. To illuminate the nanoaperture, we used circularly polarized light. The AFM mechanism was used for maintaining the sample-aperture distance on the level of several nanometres to keep the aperture in the proximity region [16].

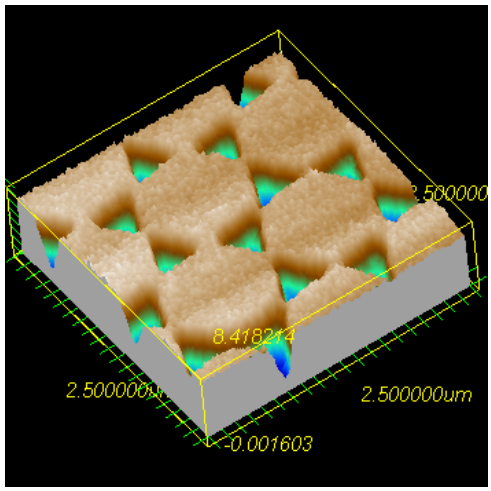

Fig. 8. 3D SNOM image of latex spheres shadows ($\phi = 1$ μm) (Al on mica)

The samples were prepared using aqueous suspension of polystyrene latex spheres [17]. We used triply distilled water with SDS (0.0025% sodium dodecyl sulfate) as a surfactant. In order to obtain a uniform layered structure of latex spheres, the surface of substrate should be hydrophilic (must be wetted by the solution). We used

a)

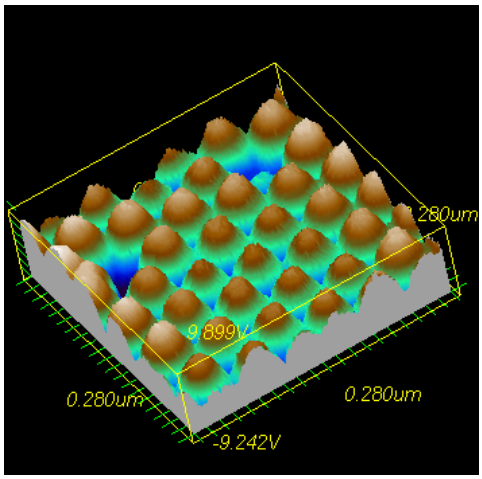

b)

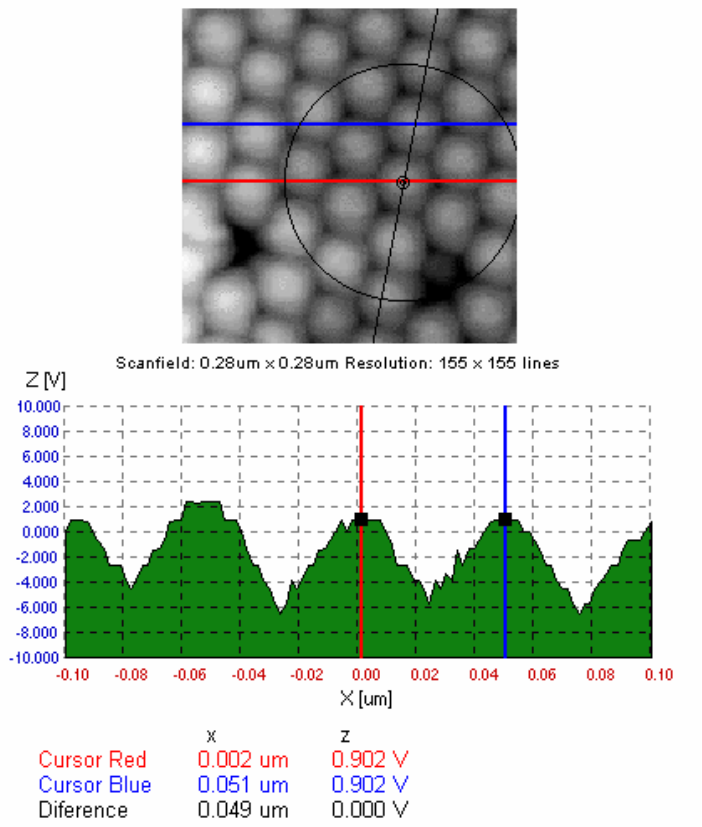

Fig. 9. 3D AFM image of latex spheres (ϕ = 50 nm) on mica (a) and measurement of sphere diameter (b)

a)

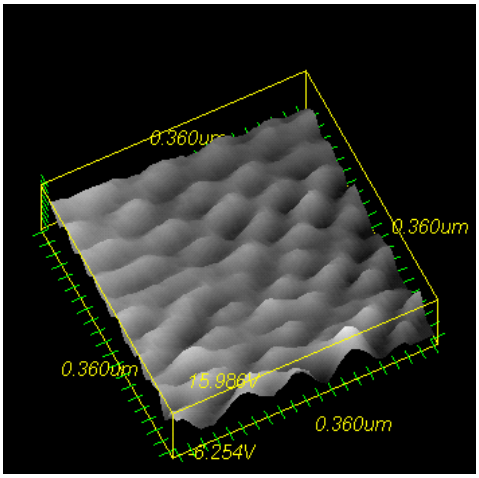

b)

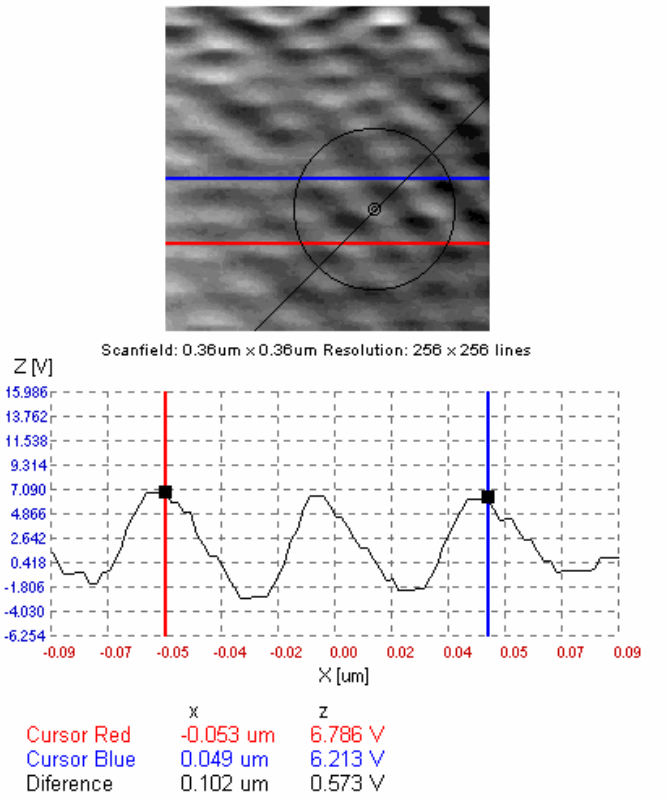

Fig 10. 3D SNOM image of latex spheres (ϕ = 50 nm) on mica (a) and measurements of sphere diameter (b)

freshly cleaved mica on which the spread-out solution forms a thin film. Upon drying at ambient temperature, the solution evaporates from the surface, the capillary force pulls the spheres together and a film of spheres is formed. In Figure 8, we show a 3D image of the shadows of the latex spheres produced by the lift-off technique. 1 μm latex spheres on the mica surface were covered with an evaporated 20 nm Al layer. The spheres were then removed with methanol in an ultrasonic bath cleaner leaving Al triangular-shaped shadows on the mica substrate. Latex spheres form a hexagonal close-packed (HCP) lattice. It is clearly seen that the optical image contains details smaller than 100 nm. To prove that, we examined a sample containing 50 nm spheres in our system. In Figure 9a, we show a 3D AFM image of such a sample. There are a few defects – vacancies of spheres visible in the image. The sphere diameter measured from the image data (Fig. 9b) equals 49 nm. In Fig. 10a, we show a 3D SNOM image of the same sample (taken in a different place on the surface). The spheres can be distinguished in the image, with edge details lost due to size of the nanoaperture used in the experiment After subsequent diameter measurements, we found the distance between the centres of the spheres equal approximately to 51 nm. The experiments performed show the ability of our system to resolve objects of the size close to the nanoaperture diameter in the optical domain.

5. Conclusions

We presented an improved method of SNOM hollow tip fabrication with nanoapertures down to 50 nm drilled using FIB. The available FIB systems equipped with *xy*-stage and image recognition allow drilling 360 sensor Cr pyramids on a wafer for reasonably short time with an excellent reproducibility (size deviation and circularity). During the measurements, we found the normalized polarization ratios between 1:77 and 1:98. Thus, a significant improvement of optical properties of our SNOM cantilevers was achieved. The transmission coefficient of nanoapertures for cone angle 50° ranges from 10^{-3} for the aperture diameter of 100 nm to 5×10^{-7} for the aperture diameter of 10 nm. In our case, we obtained 50-nm aperture throughoutput ratio of 5×10^{-5} with the values lying within 30% with respect to the polarization direction. Very good optical parameters of the fabricated cantilevers with circular apertures make them very applicable for polarity-dependent experiments which will be performed in a near future.

Acknowledgements

The authors gratefully acknowledge discussion with I.W. Rangelow. They also thank K. Domański and M. Zaborowski for help with the cantilever technology, T. Schenkel for performing FIB ion drilling of nanoapertures, and T. Gotszalk for measurements of cantilever mechanical parameters and many useful discussions. The work was partially done within the Government Project No. 4T11B00224.

References

[1] SYNGE E.H., Phil. Mag., 6, 356 (1928).
[2] POHL D.W., DENK W., LANZ M., Appl. Phys. Lett., 44 (1984), 651.
[3] LEWIS A., ISAACSON M., HAROOTUNIAN A., MURAY A., Ultramicroscopy, 13 (1984), 227.
[4] BETZIG E., TRAUTMAN J.K., Science, 257 (1992), 189.
[5] VAN HULST N.F., SEGERINK F.B., European Microsc. Anal., Jan. 1992, 13.
[6] BETZIG E., FINN P., WEINER S., Appl. Phys. Lett., 60 (1992), 2484.
[7] GRABIEC P., GOTSZALK T., RADOJEWSKI J., EDINGER K., ABEDINOV N., RANGELOW I.W., Microelectronic Eng., 61/62 (2002), 981.
[8] BETZIG E., TRAUTMAN J.K., WEINER J.S., HARRIS T.D., WOLFE R., Appl. Opt., 31 (1992), 4563.
[9] VALASKOVIC G.A., HOLTON M., MORRISON G.H., J. Microsc., 179 (1995), 29.
[10] HUSER T., LACOSTE T., HEINZELMAN H., KITZEROW H.S., J. Chem. Phys., 108 (1998), 7876.
[11] ZHOU H., MIDHA A., BRUCHHAUS L., MILLS G., DONALDSON L., WEAVER J. M. R., J. Vac. Sci. Technol. B, 17 (1999), 1954.
[12] GOTSZALK T., GRABIEC P., RANGELOW I.W., Ultramicroscopy, 82 (2000), 39.
[13] MARTIN O.J.F., PAULUS M., J. Microscopy, 205 (2002), 147.
[14] LACOSTE T., HUSER T., PRIOLL R., HEINZELMAN H., Ultramicroscopy, 71 (1998), 333.
[15] HECHT B., SICK B., WILD U.P., DECKERT V., ZENOBI R., MARTIN O.J.F., POHL D.W., J. Chem. Phys., 112 (2000), 7761.
[16] POHL D.W., FISCHER U.CH., DUERIG U.T., SPIE, Vol. 897, *Scanning Microscopy Technologies and Applications*, 1988, 84.
[17] LI Y., LINDSAY M., Rev. Sci. Instr., 62 (1991), 2630.

Received 25 June 2003
Revised 22 August 2003